Surface plasmon hurdles leading to a strongly localized giant field enhancement on two-dimensional (2D) metallic diffraction gratings

Yoann Brûlé,[1] Guillaume Demésy,[1] Boris Gralak,[1] and Evgeny Popov[1,2,*]

[1]*Aix Marseille Université, CNRS, Centrale Marseille, Institut Fresnel UMR 7249, Fac. St. Jérôme, 13397, Marseille, France*
[2]*OSA Fellow*
[*]*e.popov@fresnel.fr*

Abstract: An extensive numerical study of diffraction of a plane monochromatic wave by a single gold cone on a plane gold substrate and by a periodical array of such cones shows formation of curls in the map of the Poynting vector. They result from the interference between the incident wave, the wave reflected by the substrate, and the field scattered by the cone(s). In case of a single cone, when going away from its base along the surface, the main contribution in the scattered field is given by the plasmon surface wave (PSW) excited on the surface. As expected, it has a predominant direction of propagation, determined by the incident wave polarization. Two particular cones with height approximately 1/6 and 1/3 of the wavelength are studied in detail, as they present the strongest absorption and field enhancement when arranged in a periodic array. While the PSW excited by the smaller single cone shows an energy flux globally directed along the substrate surface, we show that curls of the Poynting vector generated with the larger cone touch the diopter surface. At this point, their direction is opposite to the energy flow of the PSW, which is then forced to jump over the vortex regions. Arranging the cones in a two-dimensional subwavelength periodic array (diffraction grating), supporting a specular reflected order only, resonantly strengthens the field intensity at the tip of cones and leads to a field intensity enhancement of the order of 10 000 with respect to the incident wave intensity. The enhanced field is strongly localized on the rounded top of the cones. It is accompanied by a total absorption of the incident light exhibiting large angular tolerances. This strongly localized giant field enhancement can be of much interest in many applications, including fluorescence spectroscopy, label-free biosensing, surface-enhanced Raman scattering (SERS), nonlinear optical effects and photovoltaics.

OCIS codes: (050.6624) Subwavelength structures; (240.6680) Surface plasmons; (050.1950) Diffraction gratings.

#231170 - $15.00 USD Received 22 Dec 2014; revised 19 Mar 2015; accepted 24 Mar 2015; published 2 Apr 2015

References and links

1. A. Hessel and A. A. Oliner, "A new theory of Wood's anomalies on optical gratings," Appl. Opt. **4**(10), 1275–1297 (1965).
2. M. C. Hutley and D. Maystre, "The total absorption of light by a diffraction grating," Opt. Commun. **19**(3), 431–436 (1976).
3. E. Popov, "Light diffraction by relief gratings: a microscopic and macroscopic view," in *Progress in Optics,* E. Wolf, ed. (Elsevier, 1993) Vol. XXXI, pp. 139–187.
4. D. A. Weitz, T. J. Gramila, A. Z. Genack, and J. I. Gersten, "Anomalous low-frequency Raman scattering from rough metal surfaces and the origin of surface-enhanced Raman scattering," Phys. Rev. Lett. **45**(5), 355 (1980).
5. A. Wirgin and T. Lopez-Rios, "Can surface-enhanced Raman scattering be caused by waveguide resonances?" Opt. Commun. **48**(6), 416–420 (1984).
6. N. Perney, J. J. Baumerg, M. E. Zoorob, M. D. Charlton, S. Mahnkopf, and C. M. Netti, "Tuning localized plasmons in nanostructured substrates for surface-enhanced Raman scattering," Opt. Express **14**(2), 847–857 (2006).
7. R. Reinisch and M. Nevière, "Electromagnetic theory of diffraction in nonlinear optics and surface-enhanced nonlinear optical effects," Phys. Rev. B **28**(4), 1870 (1983).
8. R. Reinisch, E. Popov, and M. Nevière, "Second-harmonic-generation-induced optical bistability in prism or grating couplers," Opt. Lett. **20**(8), 854-856 (1995).
9. J. -N. Yih, Y. -M. Chu, Y. -C. Mao, W. -H. Wang, F. -C. Chien, C. -Y. Lin, K. -L. Lee, P. -K. Wei, and S. -J. Chen, "Optical waveguide biosensors constructed with subwavelength gratings," Appl. Opt. **45**(9), 1938–1942 (2006).
10. E. Popov and L. Tsonev, "Electromagnetic field enhancement in deep metallic gratings," Opt. Commun. **69**(3), 193–198 (1989).
11. E. Popov, J. Wenger, J. Hoose, and S. Tonchev, "Strong three-dimensional field localization and enhancement on deep sinusoidal gratings with two-dimensional periodicity," Opt. Lett. **38**(22), 4876–4879 (2013).
12. F. J. Garcia-Vidal, J. Sánchez-Dehesa, A. Dechelette, E. Bustarret, T. López-Rios, T. Fournier, and B. Pannetier, "Localized surface plasmons in lamellar metallic gratings," J. Lightwave Technol. **17**(11), 2191–2195 (1999).
13. E. Popov, N. Bonod, and S. Enoch, "Comparison of plasmon surface waves on shallow and deep metallic 1D and 2D gratings," Opt. Express **15**(7), 4224–4237 (2007).
14. L. Langguth and A. Femius Koenderink, "Simple model for plasmon enhanced fluorescence correlation spectroscopy," Opt. Express **22**(13), 15397–15409 (2014).
15. P. J. Schuck, D. P. Fromm, A. Sundaramurthy, G. S. Kino, and W. E. Moerner, "Improving the mismatch between light and nanoscale objects with Gold bowtie nanoantennas," Phys. Rev. Lett. **94**(1), 017402 (2005).
16. E. Hao and G. C. Schatz, "Electromagnetic fields around silver nanoparticles and dimers," J. Chem. Phys. **120**(1), 357–366 (2004).
17. G. Demésy, F. Zolla, A. Nicolet, and M. Commandré, "All-purpose finite element formulation for arbitrarily shaped crossed-gratings embedded in a multilayered stack," J. Opt. Soc. Am. A **27**(4), 878–889 (2010).
18. J. P. Berenger, "A perfectly matched layer for the absorption of electromagnetic waves," J. Comput. Phys. **114**(2), 185–200 (1994).
19. C. Geuzaine and J.-F. Remacle. "Gmsh: a three-dimensional finite element mesh generator with built-in pre- and post-processing facilities," Int. J. Numer. Meth. Eng. **79**(11), 1309–1331 (2009).
20. P. Dular, C. Geuzaine, F. Henrotte, and W. Legros, "A general environment for the treatment of discrete problems and its application to the finite element method," IEEE Trans. Magn. **34**(5), 3395–3398 (1998).
21. H. A. Bethe, "Theory of diffraction by small holes," Phys. Rev. **66**(7,8), 163–182 (1944).
22. D. E. Grupp, H. J. Lezec, T. Thio, and T. W. Ebbesen, "Beyond the Bethe limit: tunable enhanced light transmission through a single sub-wavelength aperture," Adv. Mater. **11**(10), 860–862 (1999).
23. H. T. Liu and P. Lalanne, "Microscopic theory of extraordinary optical transmission," Nature **452**(7188), 728–731 (2008).
24. E. Popov, M. Nevière, A. L. Fehrembach, and N. Bonod, "Optimization of plasmon excitation at structured apertures," Appl. Opt. **44**(29), 6141–6154 (2005).
25. A. A. Rizvi and C. H. Papas, "Power flow structures in two dimensional electromagnetic fields," Prog. Electromag. Res. PIER **29**, 261–294 (2000).
26. E. Popov, L. Tsonev, and D. Maystre, "Gratings—general properties in Littrow mount and energy flow distribution," J. Mod. Opt. **37**(3), 367–377 (1990).
27. A. Nicolet, S. Guenneau, C. Geuzaine, and F. Zolla "Modelling of electromagnetic waves in periodic media with finite elements," J. Comput. Appli. Math. **168**(1), 321–329 (2004).
28. D. Gray, *American Institute of Physics Handbook,* 2^{nd} edition (Mc Graw-Hill, 1963).
29. J. Chanderzon, M. T. Dupuis, G. Cornet, and D. Maystre, "Multicoated gratings: a differential formalism applicable in the entire optical region," J. Opt. Soc. Am. **72**(7), 839–846 (1982).
30. L. Li and J. Chanderzon, "Improvement of the coordinate transformation method for surface-relief gratings with sharp edges," J. Opt. Soc. Am. A **13**(11), 2247–2255 (1996).
31. G. Granet, "Coordinate transformation method," in *Gratings: Theory and Numeric Applications*, 2^{nd} edition rev., E. Popov, ed. (Institut Fresnel, 2014), Chap. 8.

#231170 - $15.00 USD Received 22 Dec 2014; revised 19 Mar 2015; accepted 24 Mar 2015; published 2 Apr 2015

32. R. W. Wood, "On a remarkable case of uneven distribution of light in a diffraction grating spectrum," Philos. Mag. **4**, 396–402 (1902).
33. E. Popov, N. Bonod, and S. Enoch, "Non-Bloch plasmonic stop-band in real-metal gratings," Opt. Express **15**(10), 6241–6250 (2007).
34. Lord Rayleigh O. M., "III. Note on the remarkable case of diffraction spectra described by Prof. Wood," Philos. Mag. **14**(79), 60–65 (1907).
35. U. Fano, "The theory of anomalous diffraction gratings and of quasi-stationary waves on metallic surfaces (Sommerfelds waves), J. Opt. Soc. Am. **31**(3), 213–222 (1941).

1. Introduction

For more than 50 years, it has been known that excitation of surface plasmons on a periodically slightly modulated metallic surface (shallow diffraction gratings) leads to a strong (total) light absorption [1, 2] accompanied by a strong field enhancement, of the order of 100 times the incident electric field intensity [3]. This phenomenon plays a decisive role in SERS [4–6], optical Kerr effect and second-harmonic generation [7, 8], biochemical sensing [9], photovoltaics, etc. Much less widely known is the fact that deep modulation can not only behave similarly and lead to total absorption of incident light, but also that the corresponding surface plasmon responsible for this phenomenon has a localized nature. It is accompanied by an enhancement of the electric field that exceeds the excitation of surface non-localized plasmons at shallow gratings by almost one order of magnitude. Such structures have already been investigated in the literature, having a sinusoidal profiles with a 1D or 2D periodicity [10, 11], as well as lamellar 1D or 2D profiles [12, 13]. In all these cases, the existence of the localized plasmons for deep grooves can be understood taking into account the appearance of open cavity resonances inside the grooves and their interaction with the field above. Inside the grooves, lamellar gratings can support standing TEM modes, while for sinusoidal profiles the picture is more complicated and is characterized by appearance of Poynting vector curls. An electric field intensity enhancement can exceed 600 times the incident field intensity on a 2D deep sinusoidal grating.

Various values of field intensity enhancement can be found in the literature for gold nanoantennas varying from a factor of 32, calculated for a single 100 nm diameter gold Mie sphere in [14], up to a factor $> 10^3$, as experimentally determined for a 20 nm gap bowtie antennas in [15]. A factor of the order of about 10^5 has even been calculated for silver structures with a gap of 2 nm in [16].

Aiming to a better understanding of the underlying physics, we present in this paper a comparative study of the diffraction properties of a variable-height metallic cone, single or arranged in a subwavelength diffraction (infinite) array having 2D periodicity. In our study, we start with the analysis of the diffraction by a single metallic circular cone deposited on a plane metallic surface. The cone has a rounded tip in order to avoid the edge field singularities. It is shown that the scattering mechanism (diffracted field) by a relatively small or larger (with respect to the wavelength) cone does not differ qualitatively. However, the interference between (i) the diffracted field, (ii) the unperturbed field generated by the incident wave, and (iii) the wave reflected by the plane unperturbed surface, forms patterns in the field and Poynting vector distributions that differ significantly depending on the size of the cone. In particular, for small cone heights, one observes an excitation of the classical PSW along the plane metallic surface, while above some critical cone height, the Poynting vector curls reach down to the metallic surface. At these regions, the energy flow has a direction opposite to the surface plasmon propagation, and the latter is obliged to jump over the vortex regions. In this last configuration, one observes strong localization of the electric field on the tip of the cone. If the cones are arranged in a periodic array, the periodicity contributes to a collective enhancement of the field intensity on the tips of the cones, in the same manner as for sinusoidal profiles. However, here the enhancement is 10-fold stronger and its localization in space is much more pronounced.

#231170 - $15.00 USD Received 22 Dec 2014; revised 19 Mar 2015; accepted 24 Mar 2015; published 2 Apr 2015

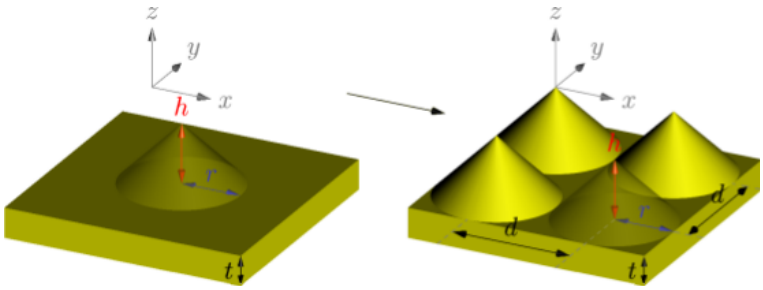

Fig. 1. Schematic representation of the simulated structures.

In the rest of the article, all the dimensions will be expressed in nanometers.

2. Poynting vector map for an unperturbed metallic plane

In order to better understand the diffraction by a single cone or a cones array, let us remind the properties of the plane wave reflected by a real-metal plane surface. Substrate is gold and the cladding air, the wavelength λ is equal to 632.8 nm, and the angle of incidence $\theta = 5.86°$ corresponds to the maximum of absorption and field enhancement for the grating in Sec.4. The incident electric field is in the plane of incidence (so-called TM polarization) and its amplitude E_0 is fixed to 1 V.m^{-1}. This plane air-gold interface can support plasmon wave for the given incident wavelength (gold refractive index is equal to $n_{Au} = 0.161952 + \mathrm{i}3.21$). Its effective index is $\alpha = k_x/k_0 = \left(\frac{n_{Au}^2}{1+n_{Au}^2}\right)^{1/2} = \alpha' + \mathrm{i}\,\alpha'' = 1.0518 + \mathrm{i}0.00567$, where k_x is the propagation constant and $k_0 = 2\pi/\lambda$ is the free-space wave number.

The electromagnetic field in the cladding is formed by the interference between the incident and the reflected plane waves. The incident plane wave is almost totally reflected (94.4% of its energy) for the given refractive index of gold and angle of incidence.

Figure 2 shows the norm and direction of the Poynting vector defined as $\mathbf{P} = \mathrm{Re}[\mathbf{E}\times\mathbf{H}^*]/2$. It can be noticed that the Poynting vector norm presents a minimum at 128 nm and 446 nm above the metallic plane surface, the separation being almost equal to half-wavelength. Its direction turns almost vertically in these regions, while being almost parallel to the surface at its maxima, where the slight inclination toward the surface represents the absorption by the real metal.

3. Field diffraction by a single cone

3.1. Geometry

The first simulated structure consists of a unique gold circular cone of height h and having a basis with a radius r, deposited on a gold slab with thickness $t = 100$ nm . The angle between the generatrice and the basis of the cone is kept equal to 40.2 deg. In order to avoid numerical artifacts due to the field singularity on the cone top, it was truncated and covered by a spherical cap of radius 7.74 nm so that the sphere tangents the truncated cone surface. We chose the specific geometry of a cone having a rounded tip in order to avoid geometries having sharp edges, and to ensure that neither the form, nor the curvature radius of the rounded tip depend on the height, as it would be the case of sinusoidal and semispherical inclusions. However, the cone form does not limit the generality of the studied phenomenon, as far as a similar behavior has already been observed in 1D and 2D sinusoidal gratings. The cladding is assumed to be air. The simulated structure is sketched in Fig. 1.

#231170 - $15.00 USD Received 22 Dec 2014; revised 19 Mar 2015; accepted 24 Mar 2015; published 2 Apr 2015

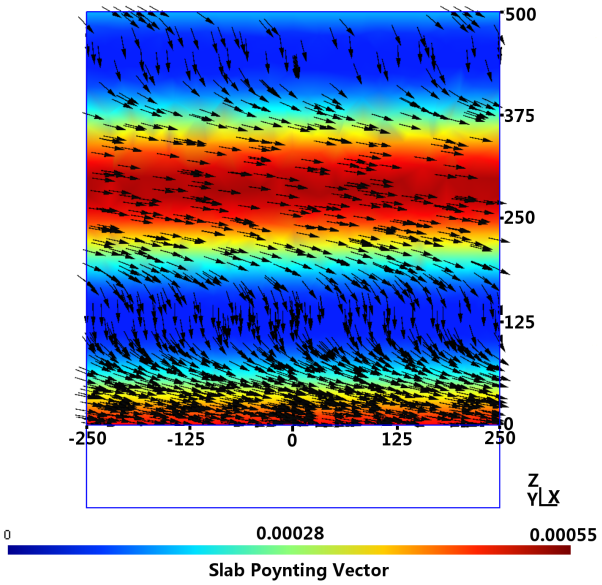

Fig. 2. Norm (color map) and direction (black arrows) of the Poynting vector in the *xz* plane for an unperturbed flat metallic surface.

3.2. *Description of the calculation method*

The simulations are performed with the finite element method (FEM). The formulation of the FEM described in [17] is used here. It allows to calculate numerically the vector field diffracted by the structure in the harmonic regime. The structure is illuminated by a plane wave of frequency ω corresponding to the wavelength $\lambda = 2\pi c/\omega$ where c is the speed of light in vacuum. The diffraction problem is treated as a radiation one by solving independently an ancillary problem, which corresponds here to the trivial diffraction problem of the slab solely. Once this problem solved, the ancillary problem solution is used as a known vectorial source term whose support is localized inside the simulated cone. Hence, the total diffracted field is the sum of three fields : (i) the so-called diffracted field calculated using the FEM, (ii) the incident plane wave, and (iii) the plane wave reflected by the plane interface (ancillary problem). It is important to note that the calculated diffracted field associated with the single cone diffraction problem satisfies an outgoing wave condition. Hence, the considered structure is embedded into a 3-dimensional box of perfectly matched layers (PMLs [18]) in order to truncate the infinite extent of the domain. The reader should refer to [17] for more details about the formulation used here. The following free softwares are used in this study: Gmsh [19] as a mesh generator and visualization tool, and GetDP [20] as a Finite Element Library.

3.3. *Electric field norm at the tip of the cone as a function of h*

Figure 3 presents the value of the norm of the total electric field (with incident electric field amplitude E_0 fixed to 1 V.m^{-1}) 1 nm above the cone tip as a function of the cone height h. From $h = 5$ nm to $h = 75$ nm, the field increases from 0.6 to 2.1, because as the cone height grows up, the total scattered field becomes stronger. After reaching a local maximum at $h = 75$ nm, further increase h up to 135 nm leads to a decay of the amplitude field maximum down to 1.2. A possible interpretation can be derived from the previous section: At a distance from the surface starting at 70 and up to 125 nm, the norm of the Poynting vector, associated to the slab problem

#231170 - $15.00 USD Received 22 Dec 2014; revised 19 Mar 2015; accepted 24 Mar 2015; published 2 Apr 2015

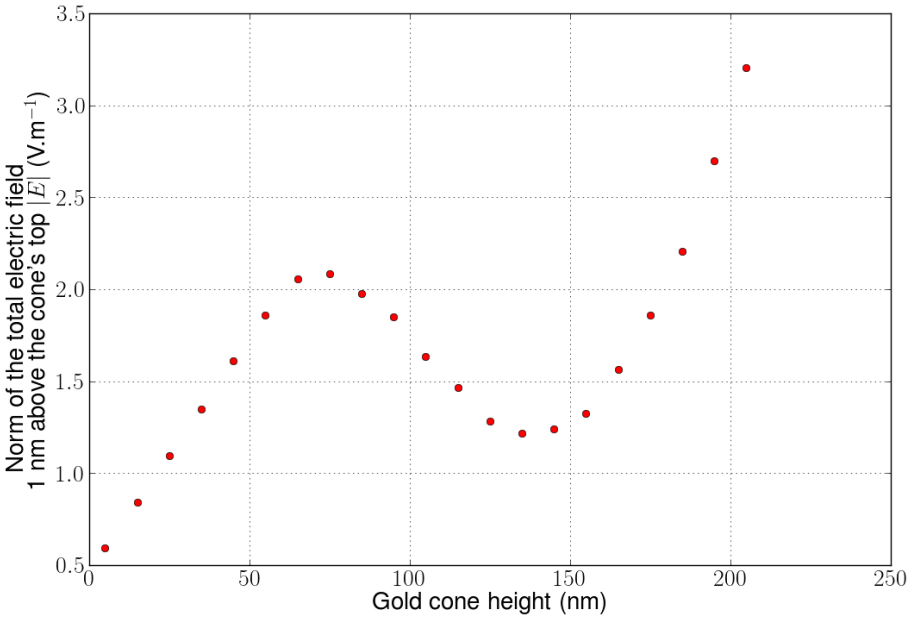

Fig. 3. Norm of the total electric field ($|E_0| = 1$ V.m^{-1}) 1 nm above the cone tip as a function of h for $\lambda = 632.8$ nm and $\theta = 5.86°$.

solely, decreases significantly. These considerations are confirmed as the cone continues to grow up to reach heights where the norm of the (slab) Poynting vector starts increasing again from $h = 135$ nm to 205 nm, and one observes another simultaneous increase of the electric field norm at the top of the cone in Fig. 3, leading to values of the field maximum up to 3.2 .

3.4. Maps of the electric field scattered by the cone

Figures 4 and 5 show the maps of the norm of the electric field scattered by the cone in presence of the slab for the two different cone heights ($h = 95$ nm and $h = 205$ nm) inside the plane of incidence (Fig. 4) and in the transverse plane (Fig. 5 for $x = 0$ nm) for the highest cone. The scattered field is defined as the difference of the total field and the unperturbed field incident and reflected by the plane slab without the cone. The direction of the corresponding scattered Poynting vector is also represented. The two height values correspond to the maxima of the local field for the grating case, as discussed later in Sec.4.

As can be observed from the scales of the colorbars in Fig. 4, the field diffracted by the cone is scattered predominantly in the xz plane, as can be expected since the incident electric field polarization lies in this very plane. In a manner similar to the diffraction by a single aperture on an infinitely conducting metallic screen, the scattered field resembles the dipole radiated field [21]. In addition to the spherical dipole field, there exists in Fig. 4 a strong field component that remains close to the slab surface and decreases rapidly when going away from the slab surface. This component cannot be observed in the transverse map (see Fig. 5). As it is well-known, in the case of real metals, the single aperture diffraction leads to excitation of PSW [22, 23]. It has a cylindrical geometry and for the existing incident polarization its azimuthal dependence is given by $\cos(\phi)$ [24], where ϕ is the azimuthal angle in the xy plane, and thus the PSW vanishes along the y-axis. These physical considerations are proved quantitatively in the next subsection.

#231170 - $15.00 USD Received 22 Dec 2014; revised 19 Mar 2015; accepted 24 Mar 2015; published 2 Apr 2015

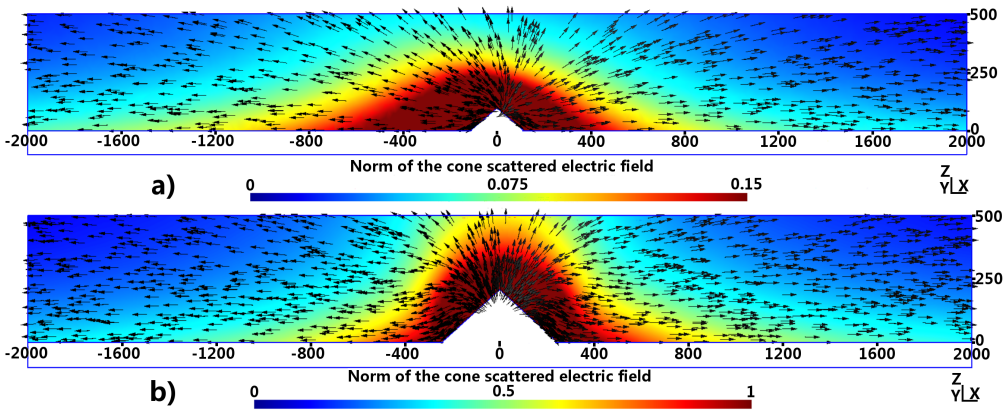

Fig. 4. Norm of the scattered electric field (colormap in V.m^{-1}) and direction of the scattered Poynting vector (black arrows) for two different cones, $h = 95$ nm (a) and $h = 205$ nm (b), in the plane $y = 0$ nm.

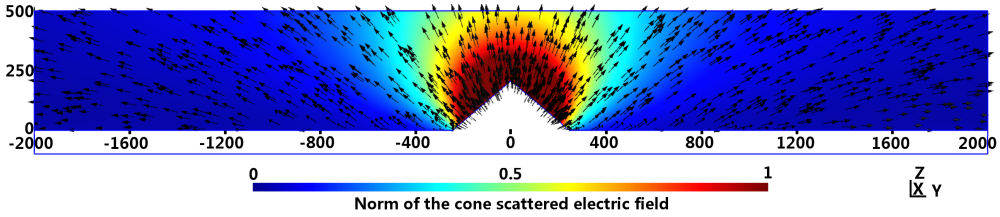

Fig. 5. Norm of the scattered electric field (colormap in V.m^{-1}) and direction of the scattered Poynting vector (black arrows) for $h = 205$ nm in the plane $x = 0$ nm.

3.5. *Surface scattered field as a plasmon surface wave*

Let us consider a quantitative data of the scattered electric field, as defined in the previous section, along the x-axis for the cone having a height of 205 nm. Its norm decreases going away from the cone base in both x and z directions, see Fig. 4. We present with a black curve in Fig. 6 the x dependence of the real part of the z component of the scattered electric field along the slab surface, 1 nm above it. Contrary to the total field norm, this representation enables to visualize not only the decay character of the field, but also its oscillating character, i.e. to determine the propagation constant of its main contribution (because there are several - the PSW, the dipole radiation, the higher-order terms due to the fact the cone is hardly a point-source dipole, etc.). As already said in the previous subsection, the field maps point to a surface wave excited predominantly in the x-direction. The general PSW theory in cylindrical geometry [24], applied in the xz plane, attributes to the PSW field z-component the first-order Hankel function H_1^+ with complex propagation constants:

$$E_{z,plasmon}(x,z) = H_1^+(k_x x)\exp(ik_z z)\,. \tag{1}$$

At the slab surface, $z = 0$ nm, the real part of E_z becomes proportional to the Bessel function of the first kind J_1:

$$\mathrm{Re}[E_{z,plasmon}]_{z=0}(x) = J_1(k_x' x)\exp(k_x'' x)\ , \tag{2}$$

having a decay constant equal to k_x''.

#231170 - $15.00 USD Received 22 Dec 2014; revised 19 Mar 2015; accepted 24 Mar 2015; published 2 Apr 2015

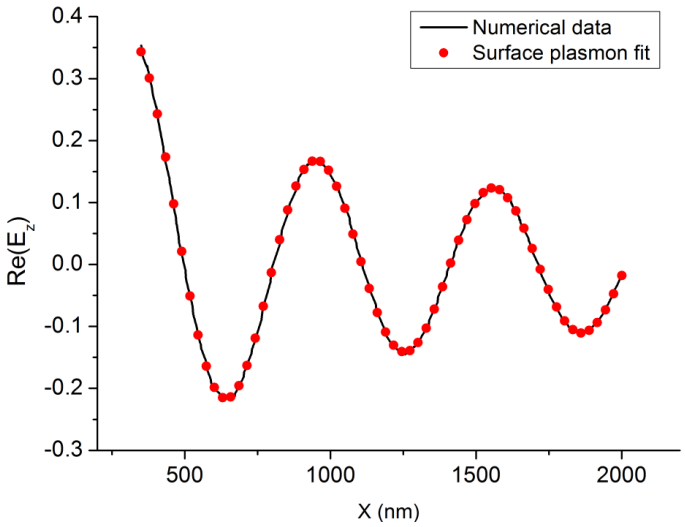

Fig. 6. z-component of the real part of the scattered electric field Re(E_z) and numerical fit with Eq. (2).

A numerical fit to the computed data for the larger cone by using the function defined in Eq. (2) gives the following results for the normalized per k_0 values of k_x: $\alpha_{fit} = \alpha' + \mathrm{i}\,\alpha'' = (1.048 \pm 0.001) + \mathrm{i}(0.005 \pm 0.0005)$. These values have to be compared to the plane slab values of Sec.2: $\alpha = \alpha' + \mathrm{i}\,\alpha'' = 1.0518 + \mathrm{i}\,0.00567$. The obvious conclusion is that the scattered field along the slab surface is majorly dominated by the PSW.

Additional information can be drawn up from the comparison of the scattered field behavior in the z-direction. A single PSW will decrease according to Eq. (1) as $\exp(ik_z z)$ with $\mathrm{Im}(k_z/k_0)$ = 0.4823, while the numerical data decay gives the value of 0.39± 0.02. Moreover, this fit gives a residual nonzero value that corresponds to the dipole radiating field, that cannot be neglected when going away from the metallic surface.

3.6. The total Poynting vector as an interference pattern between the scattered field and the unperturbed field

Figure 7 presents a cut in the plane of incidence of the total Poynting vector map for the two cones under study, with $h = 95$ nm and $h = 205$ nm. The arrows point the direction of the Poynting vector and the colormap of the arrows codes its amplitude. Both maps are striking by the appearance of Poynting vector curls, that is not quite well-known to the physical community, although being studied in detail by mathematicians in [25]. These peculiar patterns can actually be easily obtained considering only three plane waves with equal amplitudes interfering in freespace. Moreover, localized PSW on deep sinusoidal gratings have already shown such behavior [26]. Here, the pattern contains surely more than three waves, although that there are already three species ready to play the role - the incident wave, the wave reflected by the slab, and the scattered field, formed by the dipole radiation field and the PSW. Anyway, whatever the details, the result can clearly be visualized in Fig. 7.

Although their similar qualitative appearance, the Poynting vector maps for the smaller and the larger cone differ significantly in several features. The lower cone produces a total map that resembles partially an arithmetic sum of the scattered and the unperturbed Poynting vectors. In particular,

1) maximums are observed close to the surface and at a height of about 250nm,

#231170 - $15.00 USD Received 22 Dec 2014; revised 19 Mar 2015; accepted 24 Mar 2015; published 2 Apr 2015

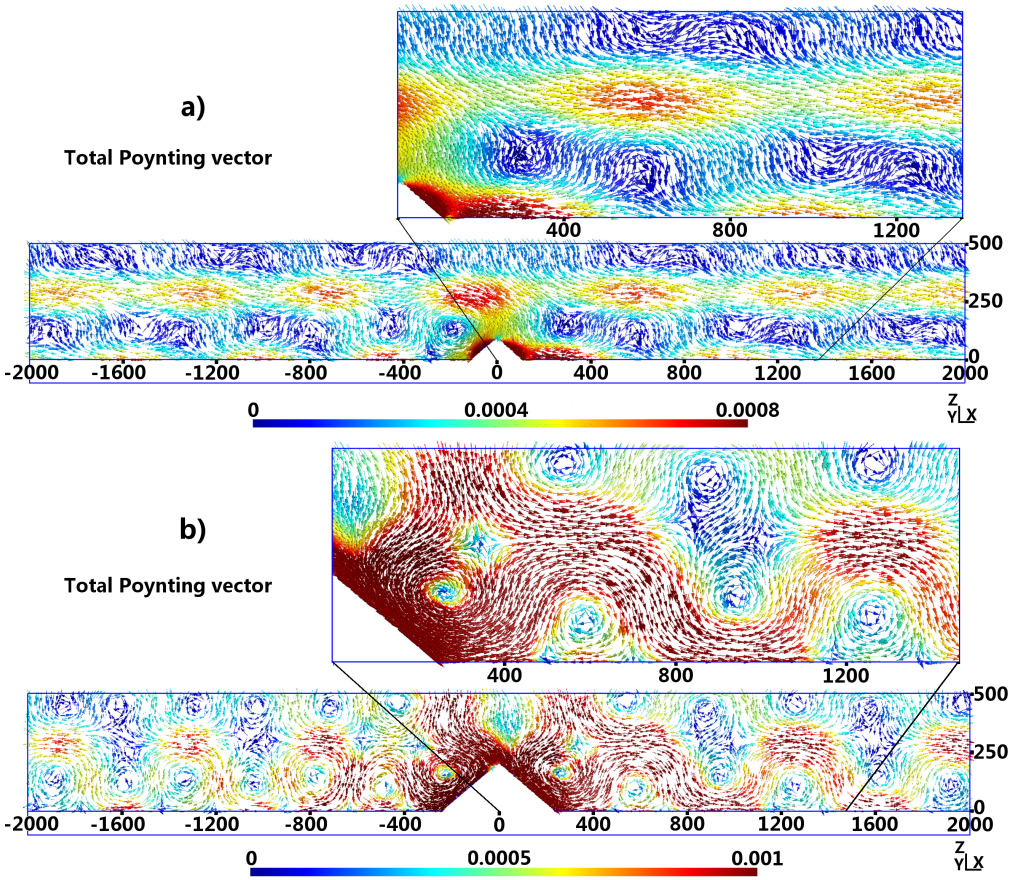

Fig. 7. Total Poynting vector for the two different cones, $h = 95$ nm (a) and $h = 205$ nm (b), in the xz-plane.

2) the two layers of maxima are separated by curls centered in the regions of minimum norm of the Poynting vector,
3) the direction of the latter is almost parallel to the slab surface, and
4) it follows the same direction on the surface ($+x$ for $x > 0$ and $-x$ for $x < 0$),
5) the lower and the upper layers of maxima are almost completely separated from each other by a layer of minima containing the vortexes.

The second map resembles the first in several points, while is completely different in others. While above points 1) to 3) still hold, a considerable change occurs for the last two:
4') **P** below the curls take an opposite direction to the PSW flow, thus there is no continuous flow touching the metal surface, and
5') the lower and the upper (close to $h = 250$ nm) maxima of the flow norm are now connected to each other, representing a continuous flux hurdling above the vortex regions.

In a few words, the observation can be summarized as follows: For the smaller cone, an excitation of the surface plasmon wave along the plane metallic surface is observed, as the total Poynting vector close to the slab is almost unidirectional and parallel to the surface. Curls of the Poynting vector are observed, formed by the interference between the cones scattered fields and the unperturbed slab fields. However, they don't perturb significantly the PSW power flow.

#231170 - $15.00 USD Received 22 Dec 2014; revised 19 Mar 2015; accepted 24 Mar 2015; published 2 Apr 2015

For the higher cone, the curls in the Poynting vector map make a direct contact with the slab metallic surface, inversing the energy flow direction at the contact regions. The surface plasmon wave has to hurdle the vortex regions and does not remain at the surface of the slab, jumping to a distance from the metal surface at a height almost equal to the cone top. This observation is important for understanding the behavior of the cone array, when they are arranged in a periodic structure.

Nevertheless, it is important to remark that with a finite-size incident beam, the field distribution of the total field outside the incident beam will contain the scattered field only. The map would correspond more or less to the map of the scattered field without the interference with the incident beam as this one is localized in space, and no plasmon hurdling will be observed for large cone outside the incident beam illuminated region.

4. Field enhancement by a periodic cones array

We have observed that a single cone with a rounded tip cannot lead to a relative intensity enhancement (only 10-fold), due to the fact that the cone is neither steep nor sharp. However, as mentioned in the introduction, when arranged in a proper manner, nanoparticles can lead to a resonant increase of the field. For a periodic array with a period d, the resonance condition is quite simple and is determined by the grating equation:

$$Re(\alpha) = \lambda/d - sin(\theta_p) \tag{3}$$

where α is the normalized resonant value of k_x as discussed in Sec. 3.5.

4.1. Geometry

The simulated gratings have a two-dimensional periodicity with $d = 500$ nm, along the two directions x and y, determined from Eq. (3) and the values of α used in Sec. 3.5. This period also ensures that the structure only supports the specular diffraction order (0,0). A unit cell of this grating is constituted of the same gold cone presented in Sec. 3.1, deposited on a 100 nm thick gold slab. Figure 1 presents a scheme of the simulated gratings.

4.2. Description of the calculation method

Under arbitrary plane wave incidence, the total field diffracted by a grating presenting two directions of periodicity is quasi-periodic along these two directions. The same FEM formulation as presented above is now used together with Bloch boundary conditions [27] along x and y instead of the lateral PML. From the calculated vector field maps, it is possible [17] to compute a complete energy balance (transmitted and reflected diffraction efficiencies and losses) of the periodic diffraction problem. This energy balance allows to check the consistency of the FEM results as the sum over all the transmitted and reflected diffraction efficiencies plus the absorption losses in dissipative parts of the grating should be equal to one. In addition, a convergence study (dependency of the calculated fields norm on the typical mesh size with respect to the wavelength) has been performed. This convergence study will not be detailed in the article but presents another verification of our results. The results have been checked against another completely independent method, based on a coordinate transformation, as explained in Sec. 4.3. As for the single cone, the incident plane wave has a wavelength λ and an incident polar angle θ. The azimuthal angle φ is kept null. The incident electric field lies in the plane of incidence (so-called TM polarization) and its amplitude E_0 is fixed to 1 V.m^{-1}. When λ is equal to 632.8 nm, the gold refractive index is taken equal to $n_{Au} = 0.161952 + i\ 3.21$. In case of dispersion (Sec. 4.3), the relative dielectric constant values for the gold can be found in [28].

#231170 - $15.00 USD Received 22 Dec 2014; revised 19 Mar 2015; accepted 24 Mar 2015; published 2 Apr 2015

4.3. *Resonant light absorption*

The geometry parameters are chosen so that a grating made of cones of height $h = 205$ nm and radius $r = 247$ nm totally absorbs the incident light at $\lambda = 632.8$ nm. As far as the grating only supports the specular reflected order, it is sufficient to look at its reflectivity only ($R_{0,0}$). Figures 8 and 9 present the results of the angular and spectral dependence of the reflectivity. The same studies are also performed with the coordinate transformation method for gratings, known as the C-method [29–31].

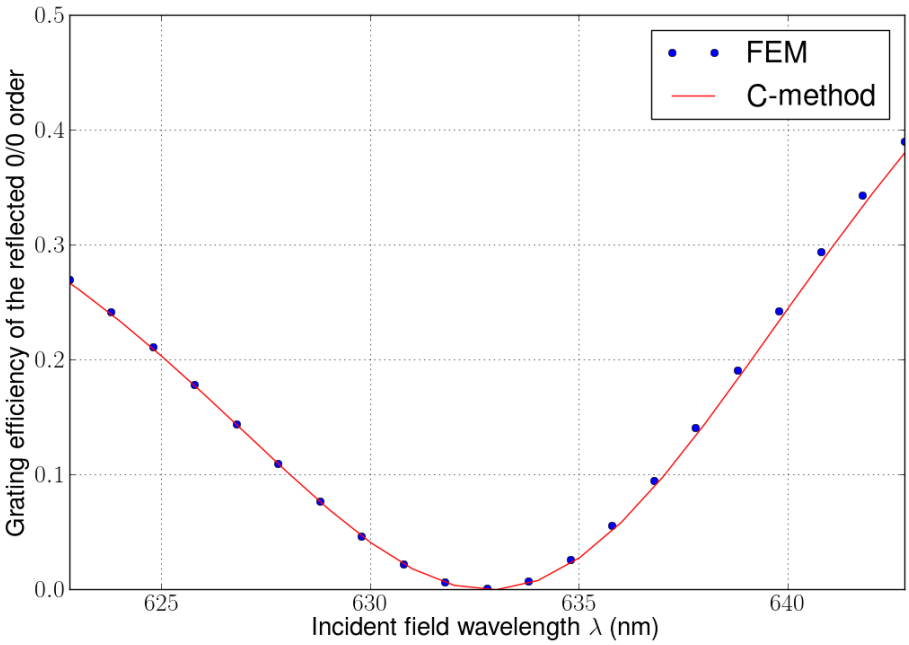

Fig. 8. Grating efficiency of the reflected specular order as a function of the incident plane wave wavelength λ, ± 10 nm around the wavelength of total absorption for $\theta = \theta_p = 5.86°$, $h = 205$ nm and $r = 247$ nm, results obtained by the FEM and the C-method.

Figure 8 presents the spectral dependency of the reflectivity around $\lambda = 632.8$ nm for an incident polar angle θ of 5.86°. A strong absorption is observed over a large spectral interval, and it reaches 100% at the resonant wavelength. The angular dependence of the reflectivity in Fig. 9, confirms that a total absorption of light occurs for $\theta = 5.86°$ and $\lambda = 632.8$ nm. Moreover, this figure confirms the observation made for plasmon resonances on deep 1D or 2D gratings: Contrary to PSW excitation on shallow gratings, the localized PSW on deep gratings are characterized by wide angular tolerances, due to the localized character of the resonance (see the field maps in the next subsection).

The same spectral and angular reflectivity curves are found by using the C-method, which confirms the consistency of the results, in addition to convergence tests and energy balance criterion.

4.4. *Giant field enhancement on a large cones array*

The reflectivity of the grating and the norm of the electric field are now studied as functions of the heights h of the cones. h spans $[5, 205]$ nm and the cones keep the same slope steepness. Figure 10 presents the results of these simulations, with the field norm values calculated at one nanometer above the cone tops.

#231170 - $15.00 USD Received 22 Dec 2014; revised 19 Mar 2015; accepted 24 Mar 2015; published 2 Apr 2015

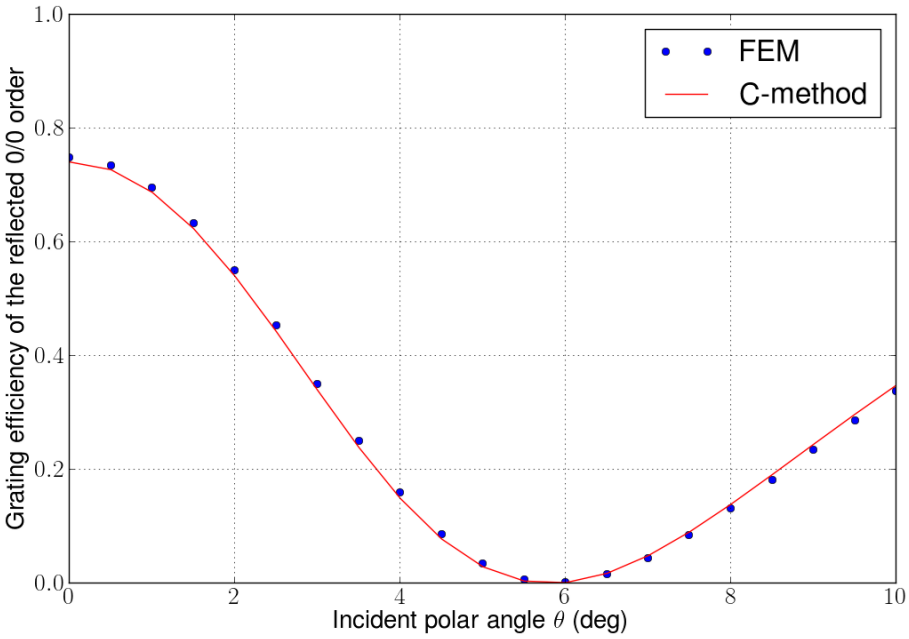

Fig. 9. Grating efficiency of the reflected specular order as a function of the incident polar angle $\theta \in [0°, 10°]$ for $\lambda = 632.8$ nm, $h = 205$ nm and $r = 247$ nm, results obtained by the FEM and the C-method.

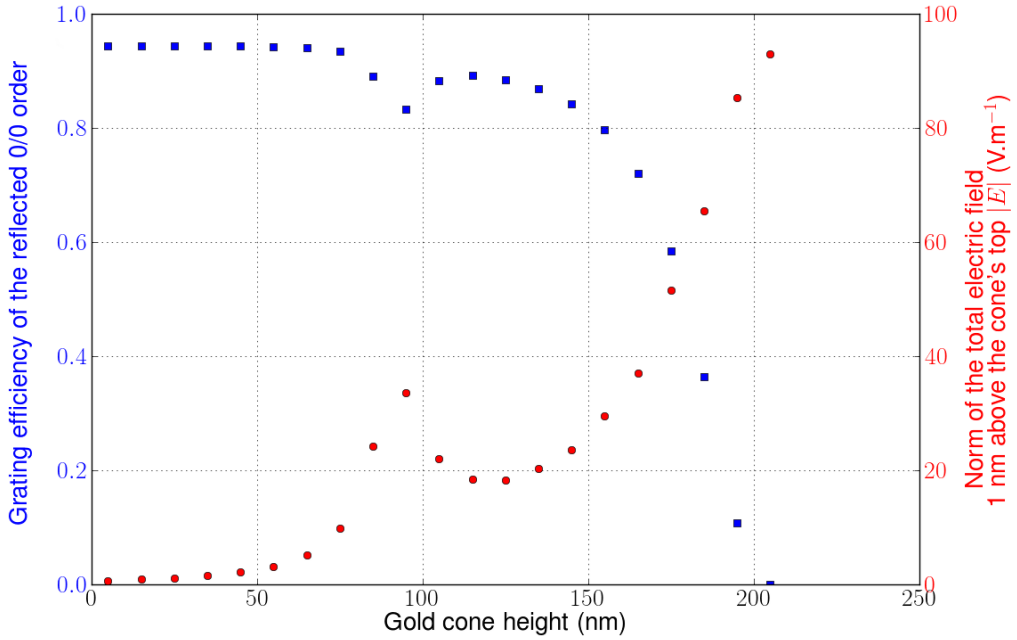

Fig. 10. Grating efficiency of the reflected specular order and norm of the total electric field 1 nm above the cone tips as a function of h for $\lambda = 632.8$ nm and $\theta = 5.86°$.

A local maximum of the field norm equal to about 34 times the incident field is observed

#231170 - $15.00 USD Received 22 Dec 2014; revised 19 Mar 2015; accepted 24 Mar 2015; published 2 Apr 2015

for h = 95 nm. It corresponds to a local minimum of reflectivity of about 83%. By varying slightly the angle of incidence, it is possible to obtain zero reflectivity. This phenomenon is known as light absorption due to resonant non-localized PSW on shallow metallic gratings, as explained in the introduction also known as Wood anomaly [32]. Further increase of the grating height increases the radiation losses of the PSW and thus its damping increases, which stops the propagation of the PSW, and it disappears [33].

A localized plasmon resonance can appear when the grating depth is increased further on, due to the appearance of open cavity resonances and their interaction with the incident electromagnetic field. In the case studied here, another enhancement of the field is observed near the second minimum of the reflectivity. A factor of 93 is obtained for the highest cone $h = 205$ nm. The C-method gives an enhancement factor of 100. These values correspond to an enhancement of 10^4 for the intensity of the field.

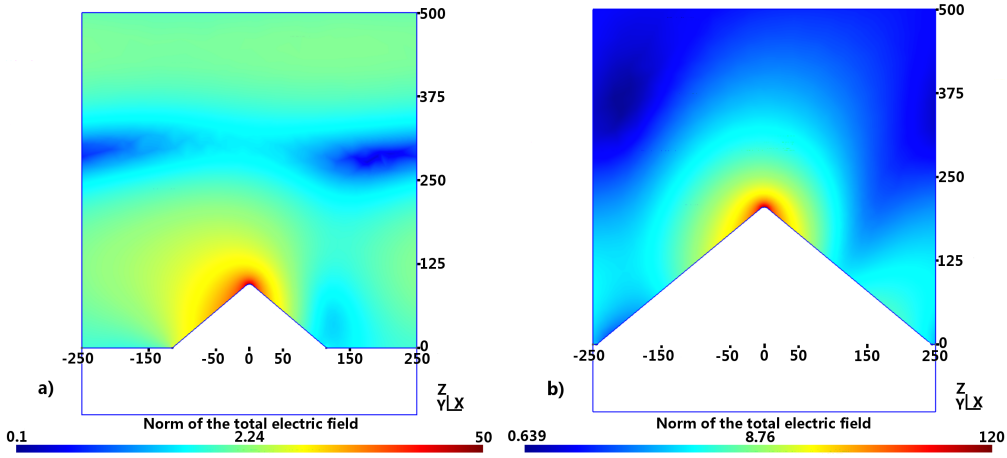

Fig. 11. Total electric field norm maps for two cones gratings of height $h = 95$ nm (a) and h = 205 nm (b), for $\lambda = 632.8$ nm and $\theta = 5.86°$ in the plane $y = 0$ nm for one cell of the gratings (colormap with a logarithmic scale).

Figure 11 presents the field maps of the total electric field norm for two height $h = 95$ nm and $h = 205$ nm. As already observed in Fig. 10 the field enhancement can reach a factor of about 50 for $h = 95$ nm and about 120 for the highest cone ($h = 205$ nm), when calculated exactly on its top. It is also observed that the field is strongly localized in z-direction, as by going away only 1 nm above the cone tips, the value of the enhancement falls to 34 for $h = 95$ nm and to 93 for $h = 205$ nm. Note that the scale of the field maps is logarithmic. In addition, the figure shows that in the horizontal direction the field for the larger cone is more strongly localized, as it decreases 10-fold within 50 nm from the cone tip, while within 100 nm for the smaller cone, thus reaching its base.

Finally, the Fourier spectrum of the total electric field for the two described cones is shown in Fig. 12. Let's remind that only the specular order (0,0) is propagating in the cladding, the higher orders being evanescent. For the smallest cones, the predominant evanescent order (-1,0) represents the PSW that propagates along the $-x$ direction, while other orders are much weaker. For the highest cones, there is no predominant diffraction order, and the electric field is less localized in the Fourier space, which reflects its stronger localization in the real space (see Fig. 11). Similar observations has been found for shallow and deep sinusoidal metallic gratings in [11].

For shallow gratings, the phenomenon is closely linked with Wood anomalies [32]. The

#231170 - $15.00 USD Received 22 Dec 2014; revised 19 Mar 2015; accepted 24 Mar 2015; published 2 Apr 2015

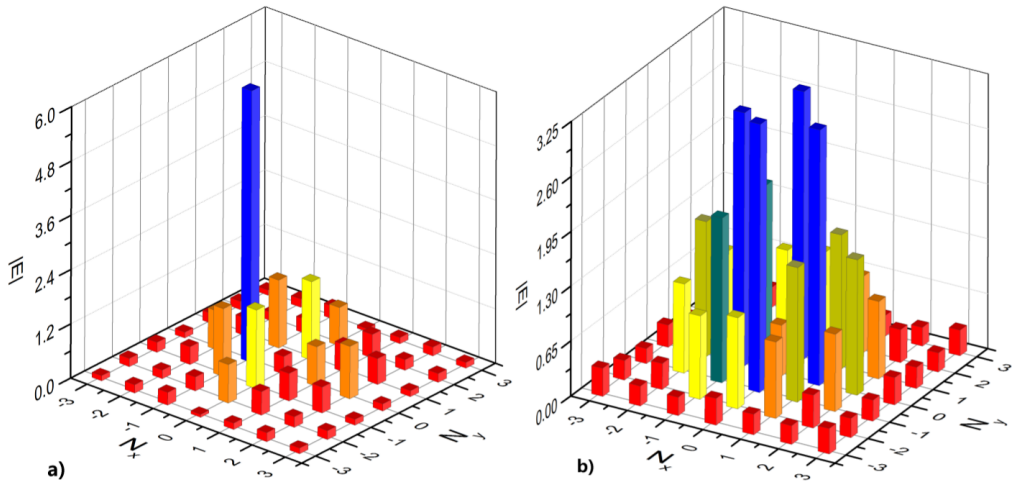

Fig. 12. Fourier decomposition (along x and y) of the total electric field vector for $h = 95$ nm (a) and $h = 205$ nm (b).

anomaly lies quite close (as a function of the angle of incidence and/or the wavelength) to the Rayleigh anomaly [34] that is due to the cut-off of the higher diffraction orders, but it is characterized by a Fano-type resonance behavior [35], due the excitation of the plasmon surface wave through the 1st diffracted order, propagating in x-direction, as becomes obvious from Fig. 12(a).

Deeper grooves lead to a localization of the surface plasmon in a small region close to the cone top, having dimensions of the order of 1/10 of the wavelength in the lateral directions (see Fig. 11(b)). The localization is also obvious in the inverse space, as it involves much larger number of evanescent Fourier harmonics, as seen in Fig. 12(b), when compared to Fig. 12(a).

4.5. Poynting vector for small and large cones

Figures 13 and 14 present the total Poynting vector maps for gratings of two different cones, $h =$ 95 nm and $h = 205$ nm. The arrows point the direction of the Poynting vector and the colormap of the arrows represents its amplitude. Figure 13 is a cut in the xz plane at $y = 0$ nm. Figure 14 is a cut in the $x + y = 0$ nm plane (diagonal plane between the two directions of periodicity). Although the figures cover a single cell of the gratings, it has to be taken into account that Poynting vector is periodic. Its amplitude is large around the cones tips. A formation of curls is observed in the near-field maps, in particular, centered at 125 nm height from the slab surface, similar to Fig. 7. In the same manner as for the diffraction by a single cone, the vortexes of the energy flow in the case of a 2D periodic array of cones separate the bottom of the grooves from their top region and thus leading to a much higher concentration of the field energy at the tops of the cones, as better observed in Fig. 14 for both smaller and larger cones. The effect is not as pronounced as for 1D sinusoidal metallic gratings where the Poynting vector is two-dimensional, while in Figs. 13 and 14 it varies in three dimensions.

4.6. Comparison with the sinusoidal grating

The total absorption of light of deep two-dimensional sinusoidal metallic gratings has already been studied in [11] and can lead to a field intensity enhancement reaching 800 times the incident intensity. The region of high intensity is strongly localized at the groove top of the grating, like in this case where the localization is at the cones tips. However, the field intensity en-

#231170 - $15.00 USD Received 22 Dec 2014; revised 19 Mar 2015; accepted 24 Mar 2015; published 2 Apr 2015

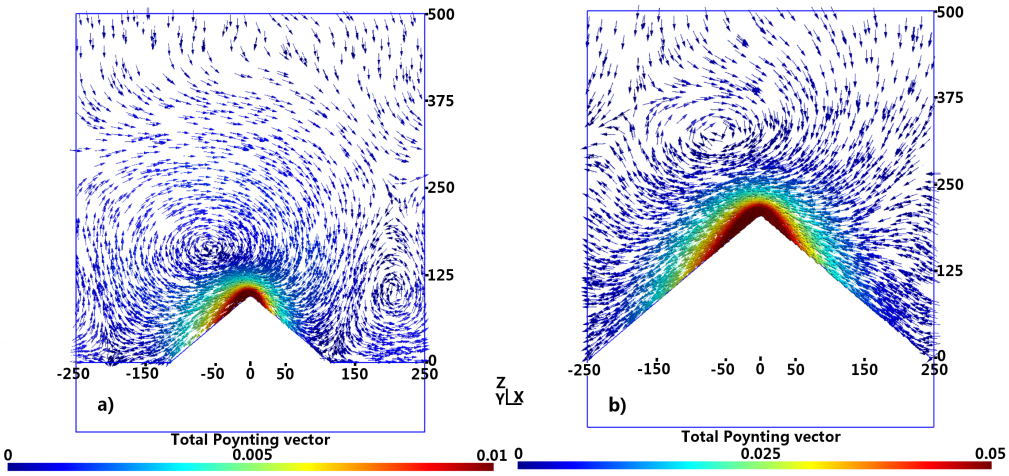

Fig. 13. Total Poynting vector for two cones gratings of height $h = 95$ nm (a) and $h = 205$ nm (b) for $\lambda = 632.8$ nm and $\theta = 5.86^\circ$ in the $y = 0$ nm plane.

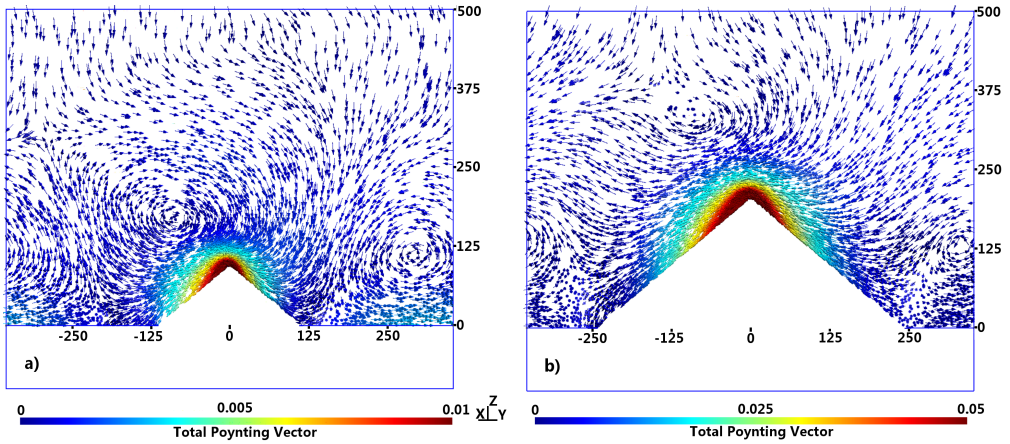

Fig. 14. Total Poynting vector for two cones gratings of height $h = 95$ nm (a) and $h = 205$ nm (b) for $\lambda = 632.8$ nm and $\theta = 5.86^\circ$ in the $x + y = 0$ nm plane.

hancement observed in this study is of a factor of 10 times higher than the one observed for two-dimensional sinusoidal gratings. In both cases, Poynting vector curls are forming inside the gratings grooves and force the plasmon surface wave to hurdle the curls from one groove's top to the other, leading to stronger field localization.

5. Conclusion

It has been shown that a periodic array of cones with rounded tips can lead to an electric field intensity that is 10 000 larger than the incident field intensity, and is strongly localized on the cones tops. This effect can be quite useful in a single-molecular detection and spectroscopy, where very small detection volumes of the order of atto-litres are welcome.

A detailed analysis of the diffraction by a single cone shows that the enhancement observed on the periodic array is due to the collective resonance caused by the periodicity of the array, as far as, for a single cone, the intensity enhancement does not exceed a factor of 10. A peculiar

#231170 - $15.00 USD Received 22 Dec 2014; revised 19 Mar 2015; accepted 24 Mar 2015; published 2 Apr 2015

behavior is found in the map of Poynting vector for a single cone with larger height, causing the flow of energy to hurdle the curls that are formed due to the interference between the incident, specularly reflected by the slab, and scattered by the cone waves. Additional study is required to see the influence of the steepness of the walls, the rounding radius of the cone, or by changing the scatterer form. For photovoltaic or sensoring application, the choice of gold as grating material limits the effect shown in this paper to red and IR; for shorter wavelength it is necessary to chose another metal. However, aluminum has a natural oxide layer 5 - 10 nm thick formed after being exposed to air, thus the field enhancement would occur mostly inside this layer. Silver has the tendency to tarnish, so that special attention has to be paid to avoid it. In addition, silver cannot support PSW in the UV.

Acknowledgments

The support of the ANR funded project PLANISSIMO (ANR-12-NANO-0003) is gratefully acknowledged.

#231170 - $15.00 USD Received 22 Dec 2014; revised 19 Mar 2015; accepted 24 Mar 2015; published 2 Apr 2015